Original Article

Multimodal imaging evaluation of early neurological deterioration following acute ischemic stroke

Meien Jiang[1,2], Guomin Li[2], Qinmeng He[2], Yulin Zhang[2], Wuming Li[2], Yunyu Gao[3], Jianhao Yan[1,2]

[1]Department of Medical Imaging, The Affiliated Guangdong Second Provincial General Hospital of Jinan University, Guangzhou, China; [2]Department of Medical Imaging, Guangdong Second Provincial General Hospital, Guangzhou, China; [3]Central Research Institute, United Imaging Healthcare, Shanghai, China

Contributions: (I) Conception and design: M Jiang, G Li, J Yan; (II) Administrative support: J Yan; (III) Provision of study materials or patients: M Jiang, Q He, Y Zhang; (IV) Collection and assembly of data: M Jiang, Q He, Y Zhang, W Li, Y Gao; (V) Data analysis and interpretation: M Jiang, G Li; (VI) Manuscript writing: All authors; (VII) Final approval of manuscript: All authors.

Correspondence to: Jianhao Yan, PhD. Department of Medical Imaging, The Affiliated Guangdong Second Provincial General Hospital of Jinan University, No. 466 Road Xingang, Guangzhou 510317, China; Department of Medical Imaging, Guangdong Second Provincial General Hospital, Guangzhou, China. Email: yanjianhao@163.com.

Background: Early neurologic deterioration occurs in up to one-third of patients with acute ischemic stroke (IS), often leading to poor functional outcomes. At present, few studies have applied amide proton transfer (APT) imaging to the evaluation of early neurological deterioration (END). This study analyzed the value of computed tomography perfusion (CTP) combined with multimodal magnetic resonance imaging (MRI) in patients with acute IS with END.

Methods: This retrospective study included patients with acute IS who were admitted to the neurology inpatient department in a tertiary hospital from October 2021 to June 2023. Patients with acute IS underwent CTP within 24 hours of stroke onset and MRI [arterial spin labeling (ASL), susceptibility-weighted imaging (SWI), and APT] within 7 days. END was defined as an elevation of ≥2 points on the National Institute of Health Stroke Scale (NIHSS) within 7 days of stroke onset. Univariable and multivariable analyses were used to compare clinical and imaging biomarkers in patients with acute IS with and without END. The performance of potential biomarkers in distinguishing between the two groups was evaluated using receiver operating characteristic (ROC) curve analysis.

Results: Among the 70 patients with acute IS, 20 (29%) had END. After conducting univariable analysis, variables were selected for entry into a binary logistic regression analysis based on our univariable analysis results, previous research findings, clinical experience, and methodological standards. The results indicated that relative cerebral blood volume (CBV) on CTP, relative cerebral blood flow (CBF) on ASL, and relative signal intensity on amide proton transfer-weighted (APTw) imaging were independent risk factors for END. The areas under the ROC curves for these risk factors were 0.710 [95% confidence interval (CI): 0.559–0.861, P=0.006], 0.839 (95% CI: 0.744–0.933, P<0.001), and 0.804 (95% CI: 0.676–0.932, P<0.001), respectively. The combined area under the curve (AUC), sensitivity, and specificity of the four indices (0.941, 100%, and 78%, respectively) were higher than those of the four indices alone.

Conclusions: CTP combined with multi-modal MRI better evaluated hemodynamics, tissue metabolism, and other relevant patient information, providing an objective basis for the clinical assessment of patients with acute IS with END and facilitating the development of accurate and personalized treatment plans.

Keywords: Early neurological deterioration (END); computed tomography perfusion (CTP); arterial spin labeling (ASL); susceptibility-weighted imaging (SWI); amide proton transfer imaging (APT imaging)

Submitted Jan 26, 2024. Accepted for publication Jun 05, 2024. Published online Jun 27, 2024.
doi: 10.21037/qims-24-153
View this article at: https://dx.doi.org/10.21037/qims-24-153

Introduction

Stroke is one of the most frequent causes of disability or death worldwide (1), among which ischemic stroke (IS) tops the list of strokes. Many patients with IS suffer worsening neurological deficits within hours or days, commonly called early neurological deterioration (END). The incidence of END ranges from 2.2% to 37.5% (2) and varies due to different definitions of END on inconsistent scales or time frames (3). As stroke patients with a too short evaluation time window may still be in the natural course of the disease, END is generally defined as an elevation of 2 points in the National Institute of Health Stroke Scale (NIHSS) within 7 days of stroke onset (4-6). At present, the etiology and pathogenesis of END in acute ischemic stroke (AIS) are unclear and complex. Several mechanisms have been suggested to account for END in AIS, including collateral failure, clot advancement, recurrent stroke, cerebral edema, seizures, hemorrhagic transformation, or re-occlusion of a recanalized artery (2,7). Among these mechanisms, hemodynamic factors (8) and tissue acid-base metabolism (9,10) may play key roles in END, contributing to infarct expansion in the same vascular territory. However, accurate, dependable, and unified early indicators to evaluate END (11) are lacking and are often difficult to identify. Therefore, exploring the relevant markers of END following AIS is of great clinical significance, especially in the early stage of treatment. Current methods for identifying individuals at high risk for END rely heavily on neuroimaging features present at the time of AIS onset, while clinical biochemical indices are of limited value in clinical application due to a lack of high sensitivity and specificity (12).

Computed tomography (CT) and magnetic resonance imaging (MRI) are widely used in clinical practice to evaluate IS and provide information about the hemodynamic status by computed tomography perfusion (CTP) imaging, micro-vessels in ischemic brain regions by susceptibility-weighted imaging (SWI), blood flow by arterial spin labeling (ASL), and acid-base metabolism and free protein production by amide proton transfer (APT). Combined imaging can accurately reflect blood perfusion and tissue metabolism in the ischemic cerebral areas in IS. Few studies have used APT to assess END following AIS. A new non-invasive magnetic resonance molecular imaging technology, amide proton transfer-weighted (APTw) imaging, uses amide protons in endogenous free proteins and free peptides in tissue cells for imaging. The exchange between endogenous amide protons and surrounding water molecules is mainly catalyzed by alkali; therefore, the exchange rate and APT signal value decrease in an acidic environment (13). A previous study (13) found that after cerebral infarction, brain tissue blood flow is higher when cerebral oxygen supply and glucose metabolism are impaired than at the time of infarction. Therefore, monitoring brain tissue blood flow may provide a sensitive indicator of early ischemia and help prevent irreversible damage. Due to the large amount of lactic acid produced by anaerobic glycolysis, ischemic tissues are affected by many factors, such as reduced bicarbonate buffer capacity, decreased perfusion, abnormal oxygen metabolism, and glucose metabolism in the acidic environment of the lesion area of stroke; the decompensation of energy metabolism in cells becomes more serious, and the pH in tissues decreases more significantly (14). As a tissue pH imaging technique, APT may be used as a biomarker reflecting abnormal tissue activity and function and can be used as a complementary means of assessing hemodynamic and structural features (14,15). Therefore, this study analyzed the value of CTP combined with multimodal MRI in patients with AIS with END. We present this article in accordance with the STROBE reporting checklist (available at https://qims.amegroups.com/article/view/10.21037/qims-24-153/rc).

Methods

Participants

The study was conducted in accordance with the Declaration of Helsinki (as revised in 2013). The study was approved by the ethics board of Guangdong Second Provincial General Hospital (No. 2023-KY-KZ-119-03), and individual consent for this retrospective analysis was waived. Patients with a preliminary clinical diagnosis of AIS between October 2021 and June 2023 were included. The other inclusion criteria were: (I) stroke in patients meeting the criteria set by the 2020 Chinese Guidelines for the Diagnosis and Treatment of AIS (16); (II) patients experiencing their first stroke onset or those with

a history of stroke but without serious sequelae (modified ranking score ≤2) (17); (III) patients with unilateral stroke >18 years of age who were admitted to the hospital within 24 h of stroke onset; (IV) infarcts ≥20 mm in size [in order to improve the accuracy and sensitivity of selecting region of interest (ROI)] showing definite hyperintensity in diffusion-weighted imaging (DWI); and (V) no serious bleeding tendencies or diseases. The exclusion criteria were: (I) inability to undergo CTP/MRI; (II) patients with brain tumors, craniocerebral trauma, psychiatric diseases, or a history of cranial surgery that may cause neurological deficits; and (III) incomplete clinical data and poor image quality (such as motion artifacts).

Clinical data (age, sex, cigarette smoking status, and medical history of hypertension, diabetes mellitus, hypercholesterolemia, atrial fibrillation, prior coronary artery disease, and prior cerebrovascular disease), treatment history, and laboratory findings (leukocyte, neutrophil, lymphocyte counts, uric acid, triglyceride, low-density lipoprotein, and high-density lipoprotein levels) were recorded. Stroke severity was assessed by two experienced neurologists (11 and 5 years of experience) independently using the NIHSS score on admission and day 7 based on the patient's medical records. The patients were divided into END and non-END groups by calculating whether the difference between the highest NIHSS score within 7 days of stroke and the NIHSS score at admission was ≥2 (4). Disagreements were resolved by consensus (for those with different scores, a consensus should be reached through mutual consultation; if no consensus can be reached, another neurologist with more than 15 years of experience should conduct the final score).

Imaging studies

All patients underwent baseline CTP on a 320-detector row CT scanner (uCT 960+, United Imaging Healthcare, Shanghai, China) within 24 h of stroke onset, including non-contrast [120 kV, 350 mA, contiguous 5-mm axial sections, matrix of 512×512, field of view (FOV) 230×230 mm^2, 7-s acquisition time, and 32 slices] and volumetric perfusion (100 kV, 75–150 mA, 5-s delay after the start of contrast medium injection, 55-s total imaging duration, 5-mm section thickness, 512×512 matrix, FOV 230×230 mm^2, and 608 slices) scanned according to our stroke imaging protocol.

All patients were scanned within seven days of stroke onset using a 3T MRI scanner (uMR 780; United Imaging Healthcare, Shanghai, China) with a 32-channel head coil. The imaging scans ranged from the parietal skull to the foramen magnum. Routine MRI examinations, including T1-fluid-attenuated inversion recovery (FLAIR), T2-FLAIR, and DWI, as well as APT, SWI, and ASL MRI, were performed. The site of cerebral infarction was determined, and other diseases were ruled out, through a routine MRI examination, including T1-weighted FLAIR (voxel size, 0.69×0.63×5.00 mm; FOV, 230 mm; repetition time, 2,221 ms; echo time, 10.2 ms; and inversion time, 960 ms, 2 min 27 s), T2-weighted FLAIR (voxel size, 1.00×0.80×5.00 mm; FOV, 230 mm; repetition time, 8,000 ms; echo time, 108.48 ms; and inversion time, 2,500 ms), and DWI (voxel size, 1.31×1.31×5.00 mm; FOV, 230 mm; four averages; b=0 and 1,000 s/mm^2; repetition time, 2,894 ms; echo time, 97.1 ms; 21 slices; and total acquisition time, 1 min 47 s) with apparent diffusion coefficient (ADC) calculation. APT imaging was performed using a single-slice two-dimensional (2D) single-shot fast spin echo (SSFSE) sequence (voxel size, 1.80×1.80×8.00 mm; FOV, 230 mm; repetition time, 4,500 ms; echo time, 39.9 ms; slice thickness, 6 mm; and slice gap, 50 mm). APTw imaging was performed employing a multi-offset approach [offsets =0, ±0.25, ±0.5, ±0.75, ±1, ±1.5, ±2, ±2.5, ±3 [2], ±3.25 [4], ±3.5 [8], ±3.75 [4], ±4 [2], ±4.5, ±5, and ±6 ppm] as part of a multi-acquisition protocol, resulting in the acquisition of 31 images. The APT sequence employed pulsed Gaussian radio frequency (RF) pulse saturation with a single saturation pulse duration of 100 ms, a duty cycle of 90%, and a power level of 2 μT. The scanning time for APT imaging was approximately 3 min 30 s, with slice positions selected to include the maximum lesion level. SWI images were acquired using a three-dimensional (3D) fast low-angle shot (FLASH) sequence (voxel size, 1.03×0.51×2.00 mm; FOV, 220 mm; repetition time, 30.20 ms; echo time, 20 ms; and acquisition time, 3 min 37 s), and post-processing included minimum intensity projection (minIP) images to assess the cerebral vessels. ASL images were acquired using a 3D pseudo-continuous ASL sequence with a 3D gradient and spin echo (GRASE) readout (voxel size, 3.50×3.50×6.00 mm; FOV, 224×224 mm^2; repetition time, 5,500 ms; echo time, 13.58 ms; labeling duration, 1,800 ms; post-labeling delay, 2,000 ms; and total acquisition time, 3 min 40 s).

Image analysis

Two experienced neuroradiologists (15 and 6 years of

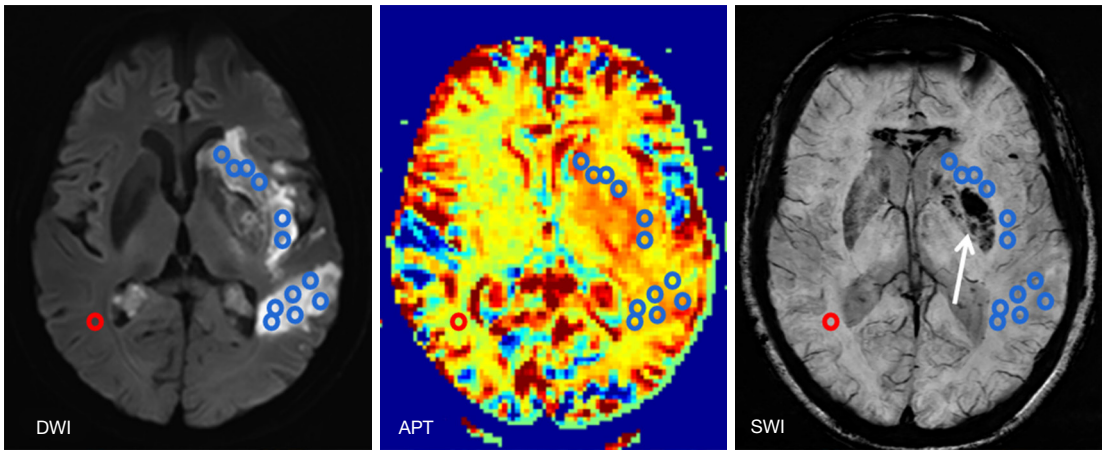

Figure 1 Example illustrating the placement of ROIs on the APT image. Twelve ROIs were positioned in the ischemic zone (blue circle), and one ROI was placed in the contralateral normal-appearing white matter (red circle), guided by the co-registered DWI and SWI images. Hemorrhagic components of lesions (white arrow) were deliberately avoided. DWI, diffusion-weighted imaging; APT, amide proton transfer; SWI, susceptibility-weighted imaging; ROI, region of interest.

experience) blinded to the patient outcomes independently observed all images and drew the corresponding ROI. Any disagreements were resolved by consensus (for those with different opinions, a consensus was reached through mutual consultation; if no consensus could be reached, another neuroradiologist with more than 20 years of experience conducted the final assessment).

All CT data were imported into the post-processing workstation (uWS-CT: R005; United Imaging Healthcare, Shanghai, China) with a fully automated processing algorithm to generate perfusion images. The largest and most obvious abnormal perfusion levels on the time to peak (TTP) images were chosen for manual delineation of the ROI. Subsequently, perfusion parameters such as cerebral blood flow (CBF), cerebral blood volume (CBV), mean transit time (MTT), TTP, and their relative values (rCBF, rCBV, rTTP, and rMTT) were measured. These measurements were then compared with those obtained from the mirrored region on the opposite side.

The measurement of ROI on MRI avoided the ventricles and sulci as much as possible. Ischemic areas were identified, and infarct volumes were measured manually on DWI imaging. On the basis of the visual assessment of the infarct volume/outcome plot, three infarct volume groups were defined (0–15, 15.1–70, and >70 mL). The largest infarct layer was selected according to the DWI findings, and the ROIs were drawn to the maximum extent in abnormal perfusion in the ASL image of the same layer. Each ROI was measured three times to obtain the average cerebral blood flow (ASL-CBF) value, and the relative cerebral blood flow (ASL-rCBF) was obtained for comparison with the CBF value of the mirror region at the same level. Based on the morphological display of the drainage veins around the infarction core area of the patients, SWI images show increased hypointensity, number, or caliber of the asymmetric medullary veins relative to the opposite side (not affected by the stroke), which is defined as the asymmetric prominent vessel sign (APVS) (18). The largest layer of cerebral infarction lesions on DWI was identified, and APT images of the corresponding layer were acquired. Hemorrhagic components of lesions were always excluded, based on the DWI and SWI co-registered with the APTw image. Each ROI was standardized to a size of 15 pixels (19), with the number of ROIs selected determined by the lesion size. The contralateral normal-appearing white matter (CNAWM) was also analyzed (*Figure 1*). For each patient, APTw values for all ROIs were recorded. The maximum (APTw max), minimum (APTw min), and mean APTw values (APTw mean) were calculated. To reduce the effects of patient age (20) and other potential experimental errors (21), we additionally recorded the relative APTw (rAPTw = APTw – APTw CNAWM).

Statistical analyses

Statistical analyses were performed using IBM SPSS

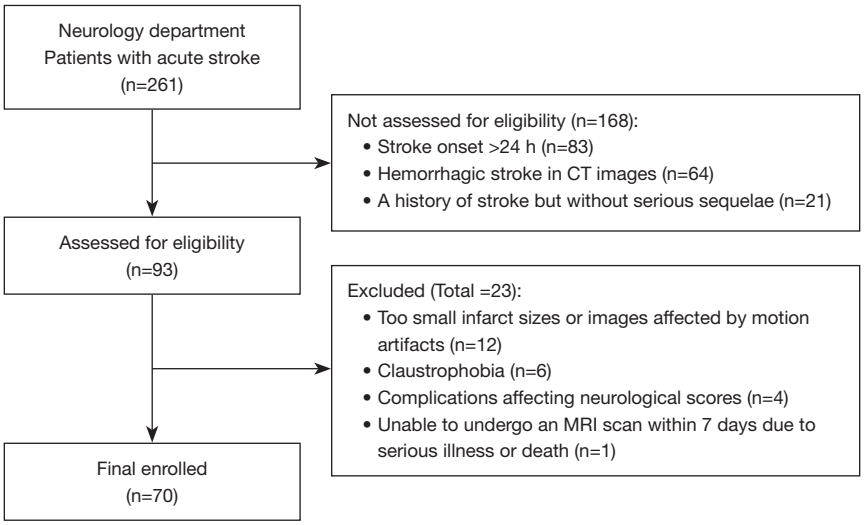

Figure 2 Follow-up flow diagram. Of 261 patients with acute stroke who were hospitalized in the neurology department, 93 patients with acute ischemic stroke who met the inclusion criteria were assessed for eligibility, and 70 (75%) were enrolled. CT, computed tomography; MRI, magnetic resonance imaging.

Statistics for Windows, version 26.0 (IBM Corp., Armonk, NY, USA). After the Shapiro-Wilk normality test, measurement data with a normal distribution were expressed as means ± standard deviation ($\bar{x}$±s), and an independent sample *t*-test was used for inter-group comparison; data with a non-normal distribution were expressed as means (quartile) and compared between two groups using non-parametric Mann-Whitney *U* tests. Counting data were expressed as percentages, and the Chi-squared test was used for comparison between groups. Single-factor analysis was used to analyze the differences between groups with or without END. Subsequently, variables were selected for inclusion in multivariable analysis to evaluate END based on the results of the univariable analysis, previous research findings (22-26), clinical experience, and methodological guidelines (27). The selected markers and their combinations were assessed through receiver operating characteristic (ROC) curves, and the area under the curve (AUC) was calculated to evaluate the performance of the selected parameters. All statistical tests were conducted as two-sided tests, with significance set at $P<0.05$ to denote statistically meaningful differences.

Results

Among the 93 patients who were initially enrolled, one was unable to undergo an MRI scan within 7 days due to serious illness or death, 12 due to infarct sizes that were too small or images affected by motion artifacts, six due to claustrophobia, and four due to complications that affect neurological scores. A total of 70 cases (mean age 63.63±1.49 years; range, 31–91 years), including 50 men (71%, 62.36±1.839 years) and 20 women (29%, 66.80± 2.386 years), who met all inclusion criteria (*Figure 2*), were included in the subsequent analysis. The median baseline NIHSS score at presentation was 6 (interquartile range: 3–9.25). Among these 70 patients, 20 (29%) developed END. The therapies included intravenous thrombolytic therapy (8 patients, 11.4%), intra-arterial thrombolysis and thrombectomy (27 patients, 38.6%), and conventional medical therapy (35 patients, 50%; 14 patients opted for conservative treatment due to their families' refusal of invasive treatment, and one case involving a high risk of intervention due to the presence of a dissecting aortic ulcerative with hematoma formation). The median infarct volume was 24.04 mL (interquartile range: 12.43–60.79 mL); 54 (77.1%) and 16 (22.9%) patients had anterior and posterior circulation strokes, respectively. According to the IS TOAST etiology classification (28), we analyzed the patients in this study and found that most patients had aortic atherosclerosis. The median time span from onset to CT examination was 6 h, ranging from 50 min to 24 h. The mean ± standard deviation (SD) of the time span from onset to MRI examination was 92 h and 18 min ± 4 h and 20 min, ranging from 20 to 168 h (approximately 0.8–7 days).

Age, sex, coronary heart disease, hypertension, hyperlipidemia, time from onset to CT/MRI examination,

and treatment method did not differ significantly between the two groups, while hyperglycemia, baseline NIHSS score, CTP-CBV, CTP-rCBV, CTP-CBF, CTP-rCBF, ASL-rCBF, SWI-APVS, APTw CNAWM, rAPTw, and infarct volume differed significantly. *Table 1* shows the outcomes in detail. In the END group, significantly more patients had diabetes (50% *vs.* 18%, P=0.007) or SWI-APVS (65% *vs.* 16%, P<0.001), and the baseline NIHSS scores (9 *vs.* 5, P=0.006) and APTw CNAWM (1.51% *vs.* 0.73%, P=0.008) were higher. The END group had significantly lower values of CTP-CBV (3.478 *vs.* 4.371 mL/100 g, P=0.021), CTP-rCBV (0.771 *vs.* 0.976, P=0.002), CTP-CBF [17.670 *vs.* 21.325 mL/(100 g·min), P=0.037], CTP-rCBF (0.609 *vs.* 0807, P=0.003), ASL-rCBF (0.380 *vs.* 0.905, P<0.001), and rAPTw (–0.553% *vs.* 0.449%, P<0.001) than the non-END group. The END group had a higher infarction volume than the non-END group (P=0.047). Binary logistic regression analysis of factors influencing END and the results showed that CTP-rCBV [odds ratio (OR) 0.719, 95% confidence interval (CI): 0.518–0.999, P=0.049], ASL-rCBF (OR 0.619, 95% CI: 0.446–0.858, P=0.004), and rAPTw (OR 0.145, 95% CI: 0.040–0.523, P=0.003) were independent factors influencing END. Collinearity diagnosis indicated no multicollinearity among the three selected variables. Univariable and multivariable analyses results used to identify AIS patients with END are presented in *Table 2*. The optimal cut-off value of the mean CTP-rCBV value in differentiating patients with and without END was 0.875, with a sensitivity of 75% and a specificity of 68%. The best cut-off value of the mean ASL-rCBF value was 0.87, the sensitivity was 100%, and the specificity was 54%. The optimal cut-off value for the average APTw value was –0.001%, with a sensitivity of 70% and a specificity of 88%. The AUC for rCBV (CTP) was 0.710 (95% CI: 0.559–0.861, P=0.006), that for ASL-rCBF was 0.839 (95% CI: 0.744–0.933,

Table 1 Clinical and imaging characteristics of patients with and without END

Variables	Non-END (n=50)	END (n=20)	P value
Demographic characteristic			
Age (years)	62.36±1.839	66.80±2.386	0.180
Sex (female:male)	15:35	5:15	0.676
Baseline NIHSS	5.00 (2.75, 8.00)	9.00 (4.25, 14.75)	0.006*
Medical history			
Hypertension	37 (74%)	15 (75%)	0.931
Diabetes	9 (18%)	10 (50%)	0.007*
Hypercholesterolemia	13 (26%)	1 (5%)	0.054
Prior coronary artery disease	11 (22%)	4 (20%)	0.854
Prior cerebrovascular disease	7 (14%)	3 (15%)	0.914
Laboratory findings			
Leukocytes (10^9/L)	8.726±2.576	9.15±2.588	0.536
Neutrophils (10^9/L)	5.67 (4.25, 8.003)	7.15 (5.008, 8.26)	0.237
Lymphocytes (10^9/L)	1.715 (1.173, 1.99)	1.425 (1.17, 2.343)	0.938
Uric acid (μmol/L)	356.98±116.842	345.8±76.682	0.695
Triglycerides (mmol/L)	1.245 (0.958, 1.968)	1.28 (0.983, 2.06)	0.965
Low density lipoprotein (mmol/L)	3.255±1.11	3.432±1.128	0.554
High density lipoprotein (mmol/L)	1.236±0.346	1.306±0.342	0.447
Time span from onset to CT examination (h)	6.5 (2.75, 21.25)	5.5 (2, 16.25)	0.535

Table 1 (*continued*)

Table 1 (*continued*)

Variables	Non-END (n=50)	END (n=20)	P value
CTP			
CBV (mL/100 g)	4.371±1.476	3.478±1.303	0.021*
rCBV	0.976±0.233	0.771±0.280	0.002*
CBF [mL/(100 g·min)]	21.325 (16.68, 25.833)	17.670 (10.65, 21.838)	0.037*
rCBF	0.807±0.233	0.609±0.227	0.003*
MTT (s)	10.914±1.386	10.783±2.137	0.762
rMTT	1.375 (1.27, 1.523)	1.365 (1.245, 1.54)	0.927
TTP (s)	28.805 (25.505, 31.820)	32.375 (27.500, 34.275)	0.140
rTTP	1.310 (1.195, 1.433)	1.400 (1.228, 1.565)	0.172
Time span from onset to MRI examination (h)	95.24±36.494	84.95±39.075	0.3
SWI-APVS	8 (16%)	13 (65%)	<0.001*
ASL-rCBF	0.905 (0.518, 1.420)	0.380 (0.223, 0.620)	<0.001*
APT			
APTw mean (%)	1.187 (0.705, 1.749)	0.793 (0.188, 1.675)	0.189
APTw min (%)	0.470±1.388	0.135±1.273	0.354
APTw max (%)	1.970 (1.138, 2.815)	1.565 (1.060, 2.635)	0.330
APTw CNAWM (%)	0.730 (0.260, 1.498)	1.510 (0.830, 2.220)	0.008*
rAPTw (%)	0.449 (0.149, 0.870)	−0.553 (−1.364, 0.218)	<0.001*
Infarction volume			0.047*
0–15 mL	19 (38%)	4 (20%)	
15.1–70 mL	23 (46%)	7 (35%)	
>70 mL	8 (16%)	9 (45%)	
Infarct location			>0.99
Anterior circulation cerebral infarct	38 (76%)	16 (80%)	
Posterior circulation cerebral infarct	12 (24%)	4 (20%)	
Treatment method			0.652
Conventional drugs	23 (46%)	12 (60%)	
Intravascular therapy	21 (42%)	6 (30%)	
Intravenous thrombolytic	6 (10%)	2 (10%)	

For continuous variables with normal distribution, the data are expressed as means ± standard deviation ($\bar{x}$ ± s). For continuous variables with non-normal distribution, the data are expressed as mean (quartile). For categorical variables, they are presented as count (percentages). *, the comparison with statistical significance (P<0.05). END, early neurological deterioration; NIHSS, National Institute of Health stroke scale; CT, computed tomography; CTP, computed tomography perfusion; CBV, cerebral blood volume; rCBV, relative cerebral blood volume; CBF, cerebral blood flow; rCBF, relative cerebral blood flow; MTT, mean transit time; rMTT, relative mean transit time; TTP, time to peak; rTTP, relative time to peak; MRI, magnetic resonance imaging; SWI-APVS, asymmetrical prominent veins sign on susceptibility-weighted imaging; ASL, arterial spin labeling; APT, amide proton transfer; APTw, amide proton transfer-weighted; APTw mean, mean APTw values; APTw max, maximum APTw values; APTw min, minimum APTw values; APTw CNAWM, APTw values of contralateral normal-appearing white matter; rAPTw, relative weighted amide proton transfer.

Table 2 Univariable and multivariable analyses to identify AIS patients with END

Variables	Univariable analysis		Multivariable analysis (step-by-step)	
	OR (95% CI)	P value	OR (95% CI)	P value
Age (years)	1.031 (0.986–1.078)	0.181		
Male	0,778 (0.239–2.529)	0.676		
Baseline NIHSS	1.169 (1.052–1.300)	0.004*		
Medical history				
Hypertension	0.949 (0.288–3.128)	0.931		
Diabetes	0.220 (0.071–0.683)	0.009*		
Hypercholesterolemia	6.676 (0.811–54.943)	0.078		
Prior coronary artery disease	1.128 (0.312–4.073)	0.854		
Prior cerebrovascular disease	0.922 (0.213–3.99)	0.914		
Laboratory findings				
Leukocytes (10^9/L)	1.067 (0.871–1.306)	0.531		
Neutrophils (10^9/L)	1.083 (0.883–1.328)	0.442		
Lymphocytes (10^9/L)	0.918 (0.462–1.824)	0.807		
Uric acid (μmol/L)	0.999 (0.994–1.004)	0.690		
Triglycerides (mmol/L)	1.070 (0.606–1.889)	0.815		
Low density lipoprotein (mmol/L)	1.157 (0.722–1.854)	0.540		
High density lipoprotein (mmol/L)	1.812 (0.398–8.247)	0.319		
Time span from onset to CT examination (h)	0.980 (0.921–1.043)	0.529		
CTP				
CBV (mL/100 g)	0.621 (0.409–0.943)	0.025*		
rCBV, per 10% change	0.672 (0.514–0.878)	0.004*	00.719 (0.518–0.999)	0.049*
CBF [mL/(100 g·min)]	0.914 (0.841–0.993)	0.034*		
rCBF, per 10% change	0.723 (0.577–0.907)	0.005*		
MTT (s)	0.950 (0.686–1.315)	0.758		
rMTT	2.184 (0.340–14.018)	0.410		
TTP (s)	1.050 (0.966–1.143)	0.252		
rTTP	4.096 (0.376–44.61)	0.247		
Time span from onset to MRI examination (h)	0.992 (0.978–1.007)	0.297		
SWI-APVS	9.750 (2.966–32.047)	<0.001*		
ASL-rCBF, per 10% change	0.655 (0.508–0.845)	0.001*	0.619 (0.446–0.858)	0.004*
APT				
APTw mean (%)	0.738 (0.453–1.203)	0.223		
APTw min (%)	0.831 (0.564–1.226)	0.351		
APTw max (%)	0.798 (0.524–1.215)	0.293		
APTw CNAWM (%)	1.657 (0.998–2.751)	0.051		
rAPTw (%)	0.203 (0.085–0.485)	<0.001*	0.145 (0.040–0.523)	0.003*

Table 2 (*continued*)

Table 2 (*continued*)

Variables	Univariable analysis		Multivariable analysis (step-by-step)	
	OR (95% CI)	P value	OR (95% CI)	P value
Infarction volume				
0–15 mL	1.000 (reference)			
15.1–70 mL	0.187 (0.044–0.789)	0.022*		
>70 mL	0.271 (0.076–0.967	0.044*		
Infarct location				
Anterior circulation cerebral infarct	1.000 (reference)			
Posterior circulation cerebral infarct	1.263 (0.354–4.513)	0.719		
Treatment method				
Conventional drugs	1.000 (reference)			
Intravascular therapy	1.565 (0.273–8.970)	0.615		
Intravenous thrombolytic	0.857 (0.136–5.395)	0.870		

*, the comparison with statistical significance (P<0.05). AIS, acute ischemic stroke; END, early neurological deterioration; OR, odds ratio; CI, confidence interval; NIHSS, National Institute of Health stroke scale; CT, computed tomography; CTP, computed tomography perfusion; CBV, cerebral blood volume; rCBV, relative cerebral blood volume; CBF, cerebral blood flow; rCBF, relative cerebral blood flow; MTT, mean transit time; rMTT, relative mean transit time; TTP, time to peak; rTTP, relative time to peak; MRI, magnetic resonance imaging; SWI-APVS, asymmetrical prominent veins sign on susceptibility-weighted imaging; ASL, arterial spin labeling; APT, amide proton transfer; APTw, amide proton transfer-weighted; APTw mean, mean APTw values; APTw max, maximum APTw values; APTw min, minimum APTw values; APTw CNAWM, APTw values of contralateral normal-appearing white matter; rAPTw, relative weighted amide proton transfer.

P<0.001), and that for rAPTw was 0.804 (95% CI: 0.676–0.932, P<0.001). Combined CTP-rCBV and ASL-rCBF: the diagnostic accuracy was significantly improved (AUC 0.872, 95% CI: 0.788–0.956, P<0.001). Combined CTP-rCBV, ASL-rCBF, and rAPTw: the diagnostic accuracy was further improved (AUC 0.941, 95% CI: 0.891–0.991, P<0.001). *Figure 3* illustrates the selected markers and their combinations for ROC curve analysis, and *Table 3* provides a comparison of the sensitivities for these parameters.

Discussion

END mainly refers to the progressive aggravation of neurological impairment symptoms in the short term after the onset of IS. This is a complex process involving multiple mechanisms, which can significantly affect the treatment prognosis and quality of life. This study showed that the incidence of neurological deterioration in patients with IS within 7 days of stroke onset was 29%, which was consistent with the 2.2–37.5% incidence reported in related studies for patients with IS in the early stage (2). A comprehensive intervention should be adopted to improve the disease prognosis of patients. Further analysis showed that clinical factors such as hyperglycemia and baseline NIHSS were closely associated with END. Previous evidence (29) has shown that sustained in-hospital hyperglycemia within 24 h after AIS is associated with a poor outcome compared with normoglycemia, which is attributed to multiple underlying mechanisms, such as vascular endothelial dysfunction, increased oxidative stress, and impaired fibrinolysis (30), leading to reduced blood perfusion in the ischemic penumbra, which in turn leads to enlarged cerebral infarct size and aggravation of the disease. The NIHSS score is a scale used to evaluate the degree of neurological deficit in stroke patients. A higher score means that the degree of cerebral ischemia and hypoxia and the degree of neurological deficit are more serious and that the tolerance is worse, which leads to an increased risk of END (31). This suggests that a high NIHSS score and hyperglycemia should be considered in the early stages of stroke. This study revealed a statistically significant difference in SWI-APVS between patients with and without END, with the presence of APVS indicating a higher risk of END in patients with IS. In cases of AIS with severe perfusion deficits, the ratio of deoxyhemoglobin to oxyhemoglobin increases (32) in the ischemic brain region, leading to venous dilation.

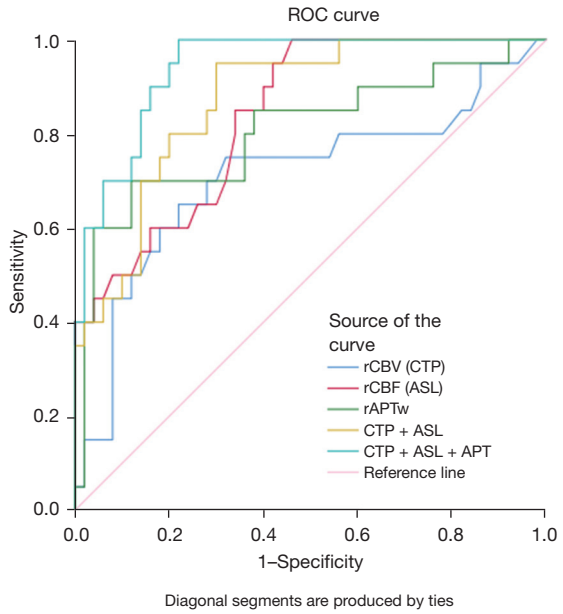

Figure 3 ROC analysis of CTP, ASL, and APT and their combination for predicting patient prognosis. The AUC for rCBV (CTP) was 0.710 (95% CI: 0.559–0.861, P=0.006), that for ASL-rCBF was 0.839 (95% CI: 0.744–0.933, P<0.001), and that for rAPTw was 0.804 (95% CI: 0.676–0.932, P<0.001). Combined CTP-rCBV and ASL-rCBF: the diagnostic accuracy was significantly improved (AUC 0.872, 95% CI: 0.788–0.956, P<0.001). Combined CTP-rCBV, ASL-rCBF, and rAPTw: the diagnostic accuracy was further improved (AUC 0.941, 95% CI: 0.891–0.991, P<0.001). ROC, receiver operating characteristic; rCBV, relative cerebral blood volume; CTP, computed tomography perfusion; rCBF, relative cerebral blood flow; ASL, arterial spin labeling; rAPTw, relative weighted amide proton transfer; APT, amide proton transfer; AUC, area under the curve; CI, confidence interval.

Consequently, the cortical veins in the affected area appear larger and exhibit lower contrast on the SWI sequence (33). The results of this study also showed that the volume of cerebral infarction was related to the occurrence of END in cerebral infarction, which was consistent with previous studies (34). The larger the infarct size, the wider the lesion area, the more serious the brain cell damage, and the higher the probability of END in patients.

This study combined a variety of imaging techniques to evaluate the hemodynamic status and tissue metabolism of cerebral ischemic areas to identify END as early as possible. Thus, patients at high risk of END can receive appropriate treatment at an early stage, thereby reducing the risk of death and improving the clinical prognosis. The results revealed significant differences in CTP-rCBV, ASL-rCBF, and rAPTw between the END and non-END groups. The average CTP-rCBV, ASL-rCBF, and rAPTw values of patients with END were lower than those of patients without END. The highest combined imaging evaluation values were observed when integrating the results from all three imaging techniques. Representative cases, illustrating both END and non-END statuses, are depicted in *Figure 4*.

A recent study (8) has suggested that infarction progression is closely related to hemodynamic and perfusion abnormalities. More obvious cerebral blood perfusion abnormalities can aggravate the degree of cerebral ischemia, increase brain tissue injury, lead to END and poor prognosis, provide quantitative data on ischemic brain areas, and effectively reflect changes in local tissue blood perfusion volume. Among CTP parameters, TTP is the most sensitive to cerebral hypoperfusion, followed by MTT. CBF is the most direct parameter, while CBV

Table 3 ROC curve analyses of the selected parameters

Parameter	AUC	Sensitivity	Specificity	Youden index	PPV	NPV
CTP-rCBV, per 10% change	0.710	75%	68%	0.43	64%	78%
ASL-rCBF, per 10% change	0.839	100%	54%	0.54	58%	82%
rAPTw	0.804	70%	88%	0.58	85%	84%
CTP + ASL	0.872	95%	70%	0.65	64%	80%
CTP + ASL + APT	0.941	100%	78%	0.78	81%	87%

ROC, receiver operating characteristic; AUC, area under the curve; PPV, positive predictive value; NPV, negative predictive value; CTP-rCBV, computed tomography perfusion relative cerebral blood volume; ASL-rCBF, arterial spin labeling relative cerebral blood flow; rAPTw, relative weighted amide proton transfer; CTP, computed tomography perfusion; ASL, arterial spin labeling; APT, amide proton transfer.

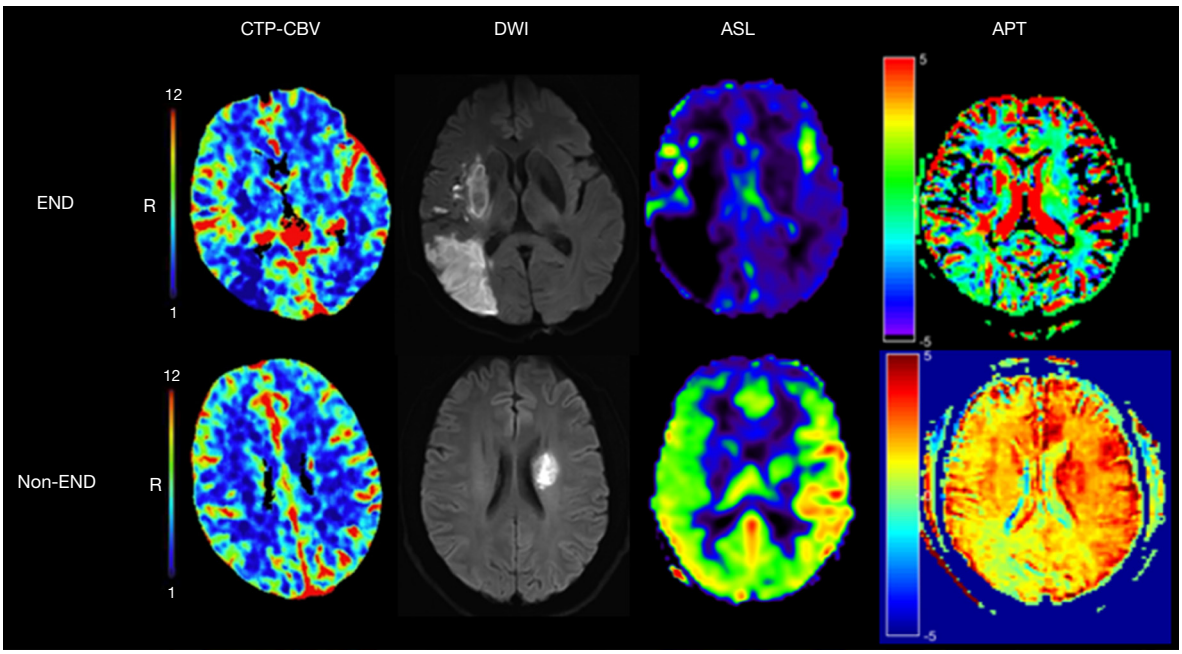

Figure 4 Representative images of patients with and without END. END: a 57-year-old man with left limb weakness for 22 hours. CTP shows obviously reduced perfusion on the right temporal lobe and basal ganglia on the CBV map. MRI shows low ASL perfusion and a decreased APTw value in the right temporal lobe and basal ganglia. The NIHSS assessment changed from 5 on admission to 13 on day 7. Non-END: a 33-year-old man with aphasia for 8 hours, CTP shows no significant decrease in perfusion on the CBV map. MRI shows high ASL perfusion and increased APTw in the left basal ganglia. The NIHSS assessment changed from 2 at admission to 1 on day 7. END, early neurological deterioration; CTP, computed tomography perfusion; CBV, cerebral blood volume; DWI, diffusion-weighted imaging; ASL, arterial spin labeling; APT, amide proton transfer; MRI, magnetic resonance imaging; APTw, amide proton transfer-weighted; NIHSS, National Institute of Health Stroke Scale.

represents compensatory capacity (35). Arenillas *et al.* (22) reported that rCBV is associated with the degree of collateral circulation. As a speculative explanation for the higher prognostic value observed for rCBV, this parameter could integrate information about both arterial and venous phases of collateral flow, thus offering a more comprehensive assessment of the viability of ischemic tissue and predicting the growth of infarction. Compared with CTP, ASL perfusion imaging directly uses water molecules in arterial blood as an endogenous tracer without injecting a contrast agent. This method is non-invasive and has strong repeatability; thus, it is more conducive to understanding changes in hemodynamics and microcirculation in cerebral ischemic areas after treatment. In their reperfusion and follow-up study, Lu *et al.* (23) showed that local high perfusion of ASL is associated with a good clinical prognosis and that ASL hyperperfusion may indicate the restoration of blood flow in the ischemic brain area or the establishment of effective collateral circulation compensation after successful reperfusion in patients with AIS. Hyperperfusion may indicate the restoration of flow to ischemic regions in patients with AIS after successful reperfusion therapy. Conversely, hypoperfusion is observed if occluded arteries are not successfully recanalized or collateral circulation is not established. This study found that pretreatment CTP combined with ASL after treatment provided a more complete estimate of ischemic tissue viability.

The results of the present study revealed a significant difference in APTw CNAWM and rAPTw values between the two groups. Binary logistic regression analysis showed that rAPT was an independent factor in evaluating END, with a lower average rAPTw value in the END group than that in the non-END group; that is, the lower APTw on the affected side was more likely to lead to END than that on the healthy side. This is similar to the findings of previous studies showing that APT-MRI can be used to determine tissue pH (36-38) and to judge the severity and prognosis of AIS in patients by assessing tissue pH metabolism (25). In

normal brain tissues, the intracellular pH is maintained at 7.2 through active and passive regulatory mechanisms (39). During ischemia, there is a reduction in blood supply to the brain. Extrusion of CO_2 from cells is limited, and glucose and oxygen supplies are reduced in patients with poor cerebral perfusion (40). As a result, bicarbonate buffering capacity decreases, and glycogen and phosphocreatine are depleted. In general, intracellular pH depends on cerebral perfusion and intracellular energy reserve time. In ischemia, brain tissue undergoes anaerobic metabolism, resulting in the accumulation of lactic acid and a decrease in pH (24,41). Worsening tissue acidification often results in cell death and damage. In addition, studies (42-44) using animal models have reported the emergence of the APT effect, where pH reduction slows the exchange of amide protons and hydrogen protons in water, while the magnetization transfer ratio (MTR) in the brain tissue of dead rats will gradually decrease. Moreover, the calibration of APT in cerebral ischemia models demonstrated obvious differences in pH values compared to unaffected brain tissues, consistent with tissue staining results (45). Thus, rAPT may be an effective marker for understanding the outcome of IS. APTw MRI is likely sensitive to intracellular acidosis in stroke, including in animal models (42-44,46) and patients (47-50), because of its sensitivity to pH changes. An increase in APTw MRI intensity indicates amelioration of intracellular acidosis or relief of brain tissue ischemia and hypoxia. This explains improvements in clinical symptoms. In contrast, a decrease in APTw MRI intensity indicates the aggravation of brain tissue ischemia and hypoxia, which would result in more serious clinical symptoms (24). As the acid-base balance of the perfusion area continues to alkalinize, the APTw reduction area shrinks, and the perfusion area correspondingly improves with the opening of the lateral branch circulation and reconstruction, resulting in a better prognosis. However, after treatment, ASL hypoperfusion remaining in the infarct indicates poor lateral branches. A decreased APTw indicates acidosis and a poor prognosis. The combination of CTP and ASL to obtain hemodynamic information before and after treatment, and then combined with APT, showed the metabolism of ischemic tissue (mainly the pH value). The combination of these three parameters can objectively display the hemodynamic status and tissue metabolism of the infarction area and provide an evidence-based assessment of END following AIS.

Each of the aforementioned imaging techniques has limitations, and a combination of multiple imaging techniques is necessary. CTP had some value in the evaluation of END in this study, as patients with lower CTP-rCBV values generally had a poor prognosis. However, patients with lower CTP-rCBV values also had a better prognosis because of recanalization after treatment (*Figure 5A*), indicating that CTP before treatment has some limitations in evaluating END. Therefore, timely image evaluation after treatment has clinical significance. The low post-treatment ASL-rCBF values (sensitivity, 100%) were the most sensitive of the four imaging techniques in this study; however, nearly half of the patients without END showed low ASL-rCBF values (*Figure 5B*). Previous studies (51,52) have shown that hyperperfusion occurs following successful vascular recanalization and tissue reperfusion because local autoregulation may take several days to adjust to the extra blood volume that tissues receive owing to the initial maximal vasodilatation caused by acute ischemia. Therefore, multiple imaging techniques should be combined to evaluate END. In addition, APT exhibited a slightly lower sensitivity (*Figure 5C*) in the assessment of END, albeit with a relatively high specificity. Even patients with high APTw showed a significant reduction in CTP-rCBV and ASL-rCBV (*Figure 5C*) and eventually developed END, which may indicate that the APTw value may be influenced not only by pH, especially in the later stages of stroke, but also by changes in the content of mobile proteins and peptides (converted amide protons) and the conventional MTR asymmetric effect (MTRasym) (53). For example, persistent energy failure caused by vessel occlusion, proteolysis, and inflammation is likely to increase mobile amides in the subacute phase, leading to an elevated APT signal (48). Therefore, the integrated use of multiple imaging techniques can improve END evaluation.

There are several limitations in this study. First, 2D APT sequences were used; therefore, only a single slice was evaluated. To mitigate potential errors, we selected the central slice with the largest infarct. In a planned future investigation, 3D APT sequences will be used as reported in the literature (54). Second, this study did not analyze other factors that may correlate with the treatment effect, such as residual stenosis or occlusion of the affected vessel(s) and the degree of diffusion-perfusion mismatch. Third, the sample size was relatively small, and the MRI scans had heterogeneous time points. Finally, our follow-up time was relatively short, and we only observed changes in the NIHSS score within seven days. Future studies will have a larger number of cases and observe stroke recurrence and

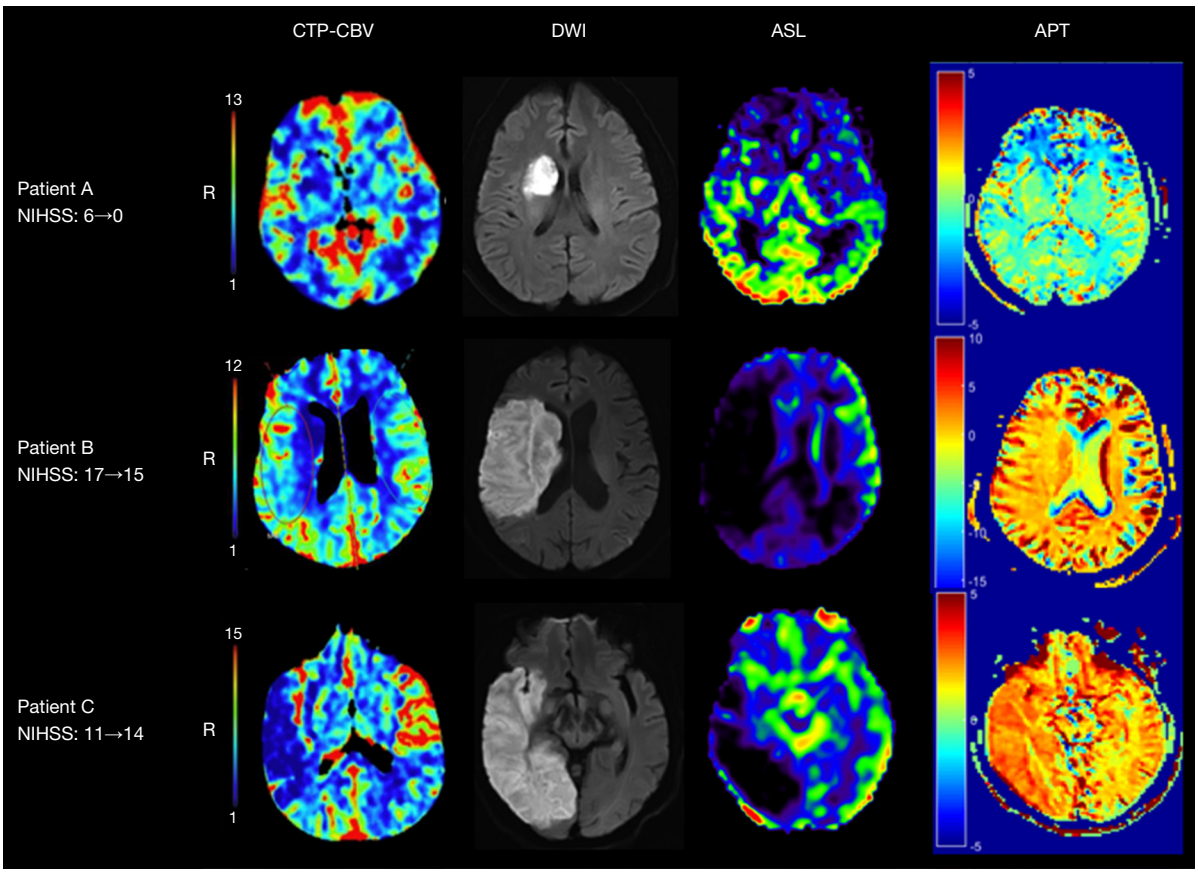

Figure 5 Images of patients without (A,B) and with (C) END showing some unexpected performance in the three informative parameters identified in this study. Patient A had lower CTP-rCBV values. After treatment, MRI showed high ASL perfusion and increased APT in the right basal ganglia; thus, the patient had a better prognosis because of recanalization. Patient B without END showed low ASL-rCBF values, probably because of the delay in local autoregulation. Patient C with END showed low CTP-rCBV and ASL-rCBF values but showed an abnormally high APT. NIHSS, National Institute of Health Stroke Scale; CTP, computed tomography perfusion; CBV, cerebral blood volume; DWI, diffusion-weighted imaging; ASL, arterial spin labeling; APT, amide proton transfer; END, early neurological deterioration; rCBV, relative cerebral blood volume; MRI, magnetic resonance imaging; rCBF, relative cerebral blood flow.

long-term prognosis.

Conclusions

Lower CTP-rCBV, ASL-rCBF, and rAPTw were associated with the occurrence of END in patients with AIS. The combined assessment of these three parameters had higher accuracy, specificity, and sensitivity compared to those for the three parameters alone. These findings suggest that these parameters can identify patients at high risk of END. This early identification can allow appropriate treatment at an early stage, thereby reducing the risk of death and improving the clinical prognosis.

Acknowledgments

Funding: None.

Footnote

Reporting Checklist: The authors have completed the STROBE reporting checklist. Available at https://qims.amegroups.com/article/view/10.21037/qims-24-153/rc

Conflicts of Interest: All authors have completed the ICMJE uniform disclosure form (available at https://qims.amegroups.com/article/view/10.21037/qims-24-153/coif). Y.G. is an employee of United Imaging Healthcare company.

The other authors have no conflicts of interest to declare.

Ethical Statement: The authors are accountable for all aspects of the work in ensuring that questions related to the accuracy or integrity of any part of the work are appropriately investigated and resolved. The study was conducted in accordance with the Declaration of Helsinki (as revised in 2013). The study was approved by ethics board of Guangdong Second Provincial General Hospital (No. 2023-KY-KZ-119-03) and individual consent for this retrospective analysis was waived.

References

1. Boursin P, Paternotte S, Dercy B, Sabben C, Maïer B. Semantics, epidemiology and semiology of stroke. Soins 2018;63:24-7.
2. Siegler JE, Boehme AK, Kumar AD, Gillette MA, Albright KC, Martin-Schild S. What change in the National Institutes of Health Stroke Scale should define neurologic deterioration in acute ischemic stroke? J Stroke Cerebrovasc Dis 2013;22:675-82.
3. Sedlaczek O, Caplan L, Hennerici M. Impaired washout--embolism and ischemic stroke: further examples and proof of concept. Cerebrovasc Dis 2005;19:396-401.
4. Kim JM, Bae JH, Park KY, Lee WJ, Byun JS, Ahn SW, Shin HW, Han SH, Yoo IH. Incidence and mechanism of early neurological deterioration after endovascular thrombectomy. J Neurol 2019;266:609-15.
5. Saver JL, Altman H. Relationship between neurologic deficit severity and final functional outcome shifts and strengthens during first hours after onset. Stroke 2012;43:1537-41.
6. Yoon CW, Park HK, Bae EK, Rha JH. Sleep Apnea and Early Neurological Deterioration in Acute Ischemic Stroke. J Stroke Cerebrovasc Dis 2020;29:104510.
7. Thanvi B, Treadwell S, Robinson T. Early neurological deterioration in acute ischaemic stroke: predictors, mechanisms and management. Postgrad Med J 2008;84:412-7.
8. Alawneh JA, Moustafa RR, Baron JC. Hemodynamic factors and perfusion abnormalities in early neurological deterioration. Stroke 2009;40:e443-50.
9. Maida CD, Daidone M, Pacinella G, Norrito RL, Pinto A, Tuttolomondo A. Diabetes and Ischemic Stroke: An Old and New Relationship an Overview of the Close Interaction between These Diseases. Int J Mol Sci 2022;23:2397.
10. Bourcier R, Goyal M, Muir KW, Desal H, Dippel DWJ, Majoie CBLM, et al. Risk factors of unexplained early neurological deterioration after treatment for ischemic stroke due to large vessel occlusion: a post hoc analysis of the HERMES study. J Neurointerv Surg 2023;15:221-6.
11. Vila N, Castillo J, Dávalos A, Chamorro A. Proinflammatory cytokines and early neurological worsening in ischemic stroke. Stroke 2000;31:2325-9.
12. Ji X, Tian L, Yao S, Han F, Niu S, Qu C. A Systematic Review of Body Fluids Biomarkers Associated With Early Neurological Deterioration Following Acute Ischemic Stroke. Front Aging Neurosci 2022;14:918473.
13. Sun PZ, Benner T, Copen WA, Sorensen AG. Early experience of translating pH-weighted MRI to image human subjects at 3 Tesla. Stroke 2010;41:S147-51.
14. Orlowski P, Chappell M, Park CS, Grau V, Payne S. Modelling of pH dynamics in brain cells after stroke. Interface Focus 2011;1:408-16.
15. Zhou J, van Zijl PC. Defining an Acidosis-Based Ischemic Penumbra from pH-Weighted MRI. Transl Stroke Res 2011;3:76-83.
16. Zhang T, Zhao J, Li X, Bai Y, Wang B, Qu Y, Li B, Zhao S; Chinese Stroke Association Stroke Council Guideline Writing Committee. Chinese Stroke Association guidelines for clinical management of cerebrovascular disorders: executive summary and 2019 update of clinical management of stroke rehabilitation. Stroke Vasc Neurol 2020;5:250-9.
17. Ni J, Yao M, Wang LH, Yu M, Li RH, Zhao LH, Wang JC, Wang YZ, Wang X, Song HQ, Luo BY, Wang JW, Huang YN, Cui LY; RESK Investigators. Human urinary kallidinogenase in acute ischemic stroke: A single-arm, multicenter, phase IV study (RESK study). CNS Neurosci Ther 2021;27:1493-503.
18. Chen CY, Chen CI, Tsai FY, Tsai PH, Chan WP. Prominent vessel sign on susceptibility-weighted imaging in acute stroke: prediction of infarct growth and clinical outcome. PLoS One 2015;10:e0131118.

19. Yu H, Lou H, Zou T, Wang X, Jiang S, Huang Z, Du Y, Jiang C, Ma L, Zhu J, He W, Rui Q, Zhou J, Wen Z. Applying protein-based amide proton transfer MR imaging to distinguish solitary brain metastases from glioblastoma. Eur Radiol 2017;27:4516-24.
20. Zhang H, Kang H, Zhao X, Jiang S, Zhang Y, Zhou J, Peng Y. Amide Proton Transfer (APT) MR imaging and Magnetization Transfer (MT) MR imaging of pediatric brain development. Eur Radiol 2016;26:3368-76.
21. Allen JS, Bruss J, Brown CK, Damasio H. Normal neuroanatomical variation due to age: the major lobes and a parcellation of the temporal region. Neurobiol Aging 2005;26:1245-60; discussion 1279-82.
22. Arenillas JF, Cortijo E, García-Bermejo P, Levy EI, Jahan R, Liebeskind D, Goyal M, Saver JL, Albers GW. Relative cerebral blood volume is associated with collateral status and infarct growth in stroke patients in SWIFT PRIME. J Cereb Blood Flow Metab 2018;38:1839-47.
23. Lu SS, Cao YZ, Su CQ, Xu XQ, Zhao LB, Jia ZY, Liu QH, Hsu YC, Liu S, Shi HB, Wu FY. Hyperperfusion on Arterial Spin Labeling MRI Predicts the 90-Day Functional Outcome After Mechanical Thrombectomy in Ischemic Stroke. J Magn Reson Imaging 2021;53:1815-22.
24. Foo LS, Harston G, Mehndiratta A, Yap WS, Hum YC, Lai KW, Mohamed Mukari SA, Mohd Zaki F, Tee YK. Clinical translation of amide proton transfer (APT) MRI for ischemic stroke: a systematic review (2003-2020). Quant Imaging Med Surg 2021;11:3797-811.
25. Lin G, Zhuang C, Shen Z, Xiao G, Chen Y, Shen Y, Zong X, Wu R. APT Weighted MRI as an Effective Imaging Protocol to Predict Clinical Outcome After Acute Ischemic Stroke. Front Neurol 2018;9:901.
26. Yu L, Chen Y, Chen M, Luo X, Jiang S, Zhang Y, Chen H, Gong T, Zhou J, Li C. Amide Proton Transfer MRI Signal as a Surrogate Biomarker of Ischemic Stroke Recovery in Patients With Supportive Treatment. Front Neurol 2019;10:104.
27. Vittinghoff E, McCulloch CE. Relaxing the rule of ten events per variable in logistic and Cox regression. Am J Epidemiol 2007;165:710-8.
28. Adams HP Jr, Bendixen BH, Kappelle LJ, Biller J, Love BB, Gordon DL, Marsh EE 3rd. Classification of subtype of acute ischemic stroke. Definitions for use in a multicenter clinical trial. TOAST. Trial of Org 10172 in Acute Stroke Treatment. Stroke 1993;24:35-41.
29. Herpich F, Rincon F. Management of Acute Ischemic Stroke. Crit Care Med 2020;48:1654-63.
30. Johnston KC, Bruno A, Pauls Q, Hall CE, Barrett KM, Barsan W, Fansler A, Van de Bruinhorst K, Janis S, Durkalski-Mauldin VL; Neurological Emergencies Treatment Trials Network and the SHINE Trial Investigators. Intensive vs Standard Treatment of Hyperglycemia and Functional Outcome in Patients With Acute Ischemic Stroke: The SHINE Randomized Clinical Trial. JAMA 2019;322:326-35.
31. Xie X, Xiao J, Wang Y, Pan L, Ma J, Deng L, Yang J, Ren L. Predictive Model of Early Neurological Deterioration in Patients with Acute Ischemic Stroke: A Retrospective Cohort Study. J Stroke Cerebrovasc Dis 2021;30:105459.
32. Xia S, Utriainen D, Tang J, Kou Z, Zheng G, Wang X, Shen W, Haacke EM, Lu G. Decreased oxygen saturation in asymmetrically prominent cortical veins in patients with cerebral ischemic stroke. Magn Reson Imaging 2014;32:1272-6.
33. Li W, Xiao WM, Luo GP, Liu YL, Qu JF, Fang XW, Wang F, Chen YK. Asymmetrical cortical vein sign predicts early neurological deterioration in acute ischemic stroke patients with severe intracranial arterial stenosis or occlusion. BMC Neurol 2020;20:331.
34. Ospel JM, Hill MD, Menon BK, Demchuk A, McTaggart R, Nogueira R, Poppe A, Haussen D, Qiu W, Mayank A, Almekhlafi M, Zerna C, Joshi M, Jayaraman M, Roy D, Rempel J, Buck B, Tymianski M, Goyal M; ESCAPE-NA1 investigators. Strength of Association between Infarct Volume and Clinical Outcome Depends on the Magnitude of Infarct Size: Results from the ESCAPE-NA1 Trial. AJNR Am J Neuroradiol 2021;42:1375-9.
35. Benson JC, Payabvash S, Mortazavi S, Zhang L, Salazar P, Hoffman B, Oswood M, McKinney AM. CT Perfusion in Acute Lacunar Stroke: Detection Capabilities Based on Infarct Location. AJNR Am J Neuroradiol 2016;37:2239-44.
36. Jokivarsi KT, Gröhn HI, Gröhn OH, Kauppinen RA. Proton transfer ratio, lactate, and intracellular pH in acute cerebral ischemia. Magn Reson Med 2007;57:647-53.
37. Zöllner JP, Hattingen E, Singer OC, Pilatus U. Changes of pH and energy state in subacute human ischemia assessed by multinuclear magnetic resonance spectroscopy. Stroke 2015;46:441-6.
38. Song G, Li C, Luo X, Zhao X, Zhang S, Zhang Y, Jiang S, Wang X, Chen Y, Chen H, Gong T, Zhou J, Chen M. Evolution of Cerebral Ischemia Assessed by Amide Proton Transfer-Weighted MRI. Front Neurol 2017;8:67.
39. Casey JR, Grinstein S, Orlowski J. Sensors and regulators of intracellular pH. Nat Rev Mol Cell Biol 2010;11:50-61.
40. Harutyunyan G, Avitsian R. Revisiting Ischemia After

Brain Injury: Oxygen May Not Be the Only Problem. J Neurosurg Anesthesiol 2020;32:5-8.
41. Ekholm A, Katsura K, Siesjö BK. Tissue lactate content and tissue PCO2 in complete brain ischaemia: implications for compartmentation of H+. Neurol Res 1991;13:74-6.
42. Jin T, Wang P, Zong X, Kim SG. Magnetic resonance imaging of the Amine-Proton EXchange (APEX) dependent contrast. Neuroimage 2012;59:1218-27.
43. Zong X, Wang P, Kim SG, Jin T. Sensitivity and source of amine-proton exchange and amide-proton transfer magnetic resonance imaging in cerebral ischemia. Magn Reson Med 2014;71:118-32.
44. McVicar N, Li AX, Gonçalves DF, Bellyou M, Meakin SO, Prado MA, Bartha R. Quantitative tissue pH measurement during cerebral ischemia using amine and amide concentration-independent detection (AACID) with MRI. J Cereb Blood Flow Metab 2014;34:690-8.
45. Heo HY, Tee YK, Harston G, Leigh R, Chappell MA. Amide proton transfer imaging in stroke. NMR Biomed 2023;36:e4734.
46. Xing C, Arai K, Lo EH, Hommel M. Pathophysiologic cascades in ischemic stroke. Int J Stroke 2012;7:378-85.
47. Zhao X, Wen Z, Huang F, Lu S, Wang X, Hu S, Zu D, Zhou J. Saturation power dependence of amide proton transfer image contrasts in human brain tumors and strokes at 3 T. Magn Reson Med 2011;66:1033-41.
48. Tietze A, Blicher J, Mikkelsen IK, Østergaard L, Strother MK, Smith SA, Donahue MJ. Assessment of ischemic penumbra in patients with hyperacute stroke using amide proton transfer (APT) chemical exchange saturation transfer (CEST) MRI. NMR Biomed 2014;27:163-74.
49. Tee YK, Harston GW, Blockley N, Okell TW, Levman J, Sheerin F, Cellerini M, Jezzard P, Kennedy J, Payne SJ, Chappell MA. Comparing different analysis methods for quantifying the MRI amide proton transfer (APT) effect in hyperacute stroke patients. NMR Biomed 2014;27:1019-29.
50. Harston GW, Tee YK, Blockley N, Okell TW, Thandeswaran S, Shaya G, Sheerin F, Cellerini M, Payne S, Jezzard P, Chappell M, Kennedy J. Identifying the ischaemic penumbra using pH-weighted magnetic resonance imaging. Brain 2015;138:36-42.
51. Deibler AR, Pollock JM, Kraft RA, Tan H, Burdette JH, Maldjian JA. Arterial spin-labeling in routine clinical practice, part 2: hypoperfusion patterns. AJNR Am J Neuroradiol 2008;29:1235-41.
52. Bivard A, Stanwell P, Levi C, Parsons M. Arterial spin labeling identifies tissue salvage and good clinical recovery after acute ischemic stroke. J Neuroimaging 2013;23:391-6.
53. Zhou J, Yan K, Zhu H. A simple model for understanding the origin of the amide proton transfer MRI signal in tissue. Appl Magn Reson 2012;42:393-402.
54. Zhou J, Zhu H, Lim M, Blair L, Quinones-Hinojosa A, Messina SA, Eberhart CG, Pomper MG, Laterra J, Barker PB, van Zijl PC, Blakeley JO. Three-dimensional amide proton transfer MR imaging of gliomas: Initial experience and comparison with gadolinium enhancement. J Magn Reson Imaging 2013;38:1119-28.

Cite this article as: Jiang M, Li G, He Q, Zhang Y, Li W, Gao Y, Yan J. Multimodal imaging evaluation of early neurological deterioration following acute ischemic stroke. Quant Imaging Med Surg 2024;14(7):4763-4778. doi: 10.21037/qims-24-153

